Title
Mechanisms for achieving high speed and efficiency in biomolecular machines

Journal
Proceedings of the National Academy of Sciences of the United States of America, 116(13)

ISSN
0027-8424

Authors
Wagoner, Jason A
Dill, Ken A

Publication Date
2019-03-26

DOI
10.1073/pnas.1812149116

Peer reviewed

Mechanisms for achieving high speed and efficiency in biomolecular machines

Jason A. Wagoner[a] and Ken A. Dill[a,b,c,1]

[a]Laufer Center for Physical and Quantitative Biology, Stony Brook University, Stony Brook, NY 11794; [b]Department of Chemistry, Stony Brook University, Stony Brook, NY 11794; and [c]Department of Physics and Astronomy, Stony Brook University, Stony Brook, NY 11794

Contributed by Ken A. Dill, January 28, 2019 (sent for review July 16, 2018; reviewed by Jonathon Howard and Daniel M. Zuckerman)

How does a biomolecular machine achieve high speed at high efficiency? We explore optimization principles using a simple two-state dynamical model. With this model, we establish physical principles—such as the optimal way to distribute free-energy changes and barriers across the machine cycle—and connect them to biological mechanisms. We find that a machine can achieve high speed without sacrificing efficiency by varying its conformational free energy to directly link the downhill, chemical energy to the uphill, mechanical work and by splitting a large work step into more numerous, smaller substeps. Experimental evidence suggests that these mechanisms are commonly used by biomolecular machines. This model is useful for exploring questions of evolution and optimization in molecular machines.

molecular machines | evolution | nonequilibrium steady state | kinetic optimization | free-energy landscape

We are interested in how biomolecular machines can be optimized for speed and efficiency. Some such machines achieve both speed and efficiency. For example, on an average day a person synthesizes, uses, and recycles his or her body weight in ATP (1, 2). All of this ATP is synthesized by the motor F_oF_1-ATPase, which achieves these results with high turnover rates [hundreds of ATPs per second per motor (3)] at high thermodynamic efficiency [$\sim$90% in animal mitochondria (4)].

For a particular machine with a fixed mechanism, going faster comes at the expense of efficiency. However, through evolution, a machine can develop mechanisms that optimize the entire speed–efficiency curve; they increase speed at no cost to efficiency or vice versa. What are these mechanisms that biomolecular machines have evolved to be both fast and efficient?

Previous studies have identified some specific mechanisms that optimize speed, such as a constant torque generation over the angular coordinate of a rotary motor (5), the evolutionary preference for a rotary mechanism in F_oF_1-ATPase (6), and a transition-state location close to the initial state of a machine's mechanical step (7–9). Other studies have found more general principles—how to best distribute the barrier heights and free-energy drops across a cyclic free-energy landscape both for molecular machines (10, 11) and for maximizing the catalytic efficiency of enzymes (12, 13). Our work is consistent with and builds on these previous results to identify the essential mechanisms for optimizing speed in molecular machines. We explore in particular how a machine can link a large downhill chemical energy to a large uphill mechanical work using intermediate conformational changes, the role of the transition-state location, and the kinetic advantage of splitting a single large work step into smaller "chunks" or substeps.

A Two-State Model of a Molecular Machine

We model how a machine converts the free energy that is put into the system, $\Delta\mu \geq 0$, into the work performed by the system, $w \geq 0$ (Fig. 1). We divide machine actions into two steps, a nonmechanical transition ($A_j \rightarrow B_j$), which may include chemical and/or conformational changes, and a mechanical transition ($B_j \rightarrow A_{j+1}$), over which it performs work. This assumes that the machine is fully coupled; i.e., there is one output step for every input step. The model is periodic: The subscript j labels the position along the track or the number of forward cycles completed.

We use this model to study a broad class of machines, including those with distinct mechanical steps (such as the transport motors kinesin and myosin) and others that have their work output delocalized or "smeared" across the entire machine cycle (such as Na-K ATPase) (14). Although it is simpler than the reaction mechanisms of these real machines, this two-state model captures many essential features of how a machine can best use its input free energy to overcome the kinetic barriers of performing large uphill work.

Expressing Model Mechanisms with Basic Free-Energy Diagrams. For illustrating mechanisms in this paper, we use diagrams of free-energy–like functions. But first, we describe what our diagrams mean. The observable quantities in Fig. 1 are the forward and reverse rates. We represent these rates in terms of the following free-energy barrier definitions,

$$f_c = k_0\, e^{-\beta g^{\ddagger}_{fc}} \qquad r_c = k_0\, e^{-\beta g^{\ddagger}_{rc}}$$
$$f_m = k_0\, e^{-\beta g^{\ddagger}_{fm}} \qquad r_m = k_0\, e^{-\beta g^{\ddagger}_{rm}}, \qquad [1]$$

where k_0 is a frequency factor and the free-energy barriers $g^{\ddagger}_{fc}$, etc., are defined to be positive.

Significance

Molecular machines are cellular proteins that transduce energy. They can convert energy to motion, recharge ATP stores by harnessing ion flows, and pump ions energetically uphill. Molecular machines are able to be both fast and efficient at the same time. How do they achieve high speeds at high efficiency? Here we explore mechanisms of evolution or synthetic design that can optimize these properties, such as a conformationally driven mechanical step, which varies the conformational free-energy landscape to mitigate large kinetic barriers, and mechanical substeps, which split one large kinetic barrier into multiple smaller ones.

Author contributions: J.A.W. and K.A.D. designed research; J.A.W. performed research; J.A.W. analyzed data; and J.A.W. and K.A.D. wrote the paper.

Reviewers: J.H., Yale University; and D.M.Z., Oregon Health & Science University.

The authors declare no conflict of interest.

[1]To whom correspondence should be addressed. Email: dill@laufercenter.org.

This article contains supporting information online at www.pnas.org/lookup/suppl/doi:10.1073/pnas.1812149116/-/DCSupplemental.

Published online March 8, 2019.

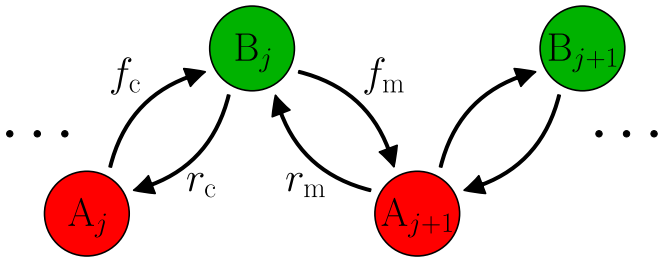

Fig. 1. The machine cycle is divided into two steps: one nonmechanical (c) and one mechanical (m). The mechanical step ($B_j \rightarrow A_{j+1}$) generates the output of a machine and performs work (e.g., the stepping of kinesin along a microtubule). The nonmechanical step ($A_j \rightarrow B_j$) includes chemical or conformational changes of the machine that do not perform work.

Now, if our machines were at equilibrium, we could illustrate their properties using standard free-energy diagrams based on expressions such as

$$\frac{f_c f_m}{r_c r_m} = e^{-\beta\left(g_{c,eq}+g_{m,eq}\right)} = 1, \qquad [2]$$

where $g_{c,eq}$, $g_{m,eq}$ are the equilibrium free-energy changes between the states. Since these are cyclic processes, the free energies must sum to zero around an equilibrium cycle; i.e., $(g_{c,eq} + g_{m,eq}) = 0$.

However, here we are interested in steady-state processes, not at equilibrium. But we can capture insights using similar expressions such as

$$\frac{f_c f_m}{r_c r_m} = e^{-\beta(g_c+g_m)} = e^{\beta(\Delta\mu - w)} = e^{\beta\Delta\mu_{diss}}. \qquad [3]$$

Here, $\Delta\mu$ is a chemical work that is done on the system and w is a work done by the system. Their difference, $(\Delta\mu - w) = \Delta\mu_{diss} \geq 0$, is a dissipation of heat and due to differences in concentrations of reactants (ATP) and products (ADP and P_i), which constrains the forward and reverse rates in Eq. **3** (15–17). So, the quantities g_c and g_m are not true equilibrium free-energy differences between states A and B. Instead, these quantities give the changes in basic free energy shown in Fig. 2. The basic free energy is an analog of an equilibrium free energy that is corrected for nonequilibrium effects, such as a difference in chemical potentials of species that are out of equilibrium (e.g., [ATP]), to give an equivalent kinetic and thermodynamic formalism (15). Eq. **3** shows that, across a full cycle, these quantities are constrained by the measured observables $\Delta\mu$ and w: $g_c + g_m = -(\Delta\mu - w) = -\Delta\mu_{diss}$. We hope these basic free-energy landscapes are helpful for illustrating mechanisms below.

Now, in terms of the rate coefficients above, we can compute the cycle flux (number of full cycles per unit time) as (*SI Appendix*, section 1)

$$J = \frac{f_c f_m - r_c r_m}{f_c + f_m + r_c + r_m}. \qquad [4]$$

For a cytoskeletal walker, the velocity is $V = Jd$ for step size d. For an ion pump that transports n ions per cycle, the current $I = nJ$. We use "speed" to refer to these quantities (flux, velocity, or current). We define the thermodynamic efficiency of a machine as

$$\eta = \frac{w}{\Delta\mu}. \qquad [5]$$

Defining Parameters for the Free-Energy Transduction Across the Machine Cycle. The machine landscape in Fig. 2 is defined by the four barrier heights $g^{\ddagger}$ and the basic free-energy changes g_c and g_m. For any given pair of macroscopic observables $\Delta\mu$ and w, there are many possible ways to define these quantities. Here, we define three parameters λ, δ, and N that represent essential features of this landscape and of the machine's free-energy transduction. We then explore machine optimization principles over these parameters.

First, let λ be the fraction of free energy from the input chemical work that is expended within the mechanical step. Thus, $1 - \lambda$ is the fraction expended across the nonmechanical step:

$$\begin{aligned} g_c &= g^{\ddagger}_{fc} - g^{\ddagger}_{rc} = -(1-\lambda)\Delta\mu \\ g_m &= g^{\ddagger}_{fm} - g^{\ddagger}_{rm} = -\lambda\Delta\mu + w. \end{aligned} \qquad [6]$$

This quantity λ describes an inherent feature of the machine cycle, independent of w, and implicitly includes two contributions, from the input chemical energy $\Delta\mu$ and from changes in conformational free energy, which must sum to zero across the full cycle. In short, when $\lambda = 0$, the decrease in basic free energy that is available from input chemical energy is expended in the first, nonmechanical step ($g_c = -\Delta\mu$) and all of the work is performed in the mechanical step ($g_m = w$). In contrast, when $\lambda = 1$, there is no change in basic free energy across the first step ($g_c = 0$) and all of the energetic changes happen in the second step ($g_m = -\Delta\mu + w = -\Delta\mu_{diss}$) (Fig. 3*A*).

Second, let δ represent the location of the transition state along the mechanical step, which dictates how a change in w will affect the forward $g^{\ddagger}_{fm}$ and reverse $g^{\ddagger}_{rm}$ barrier heights (7–9). Together, λ and δ define the barrier heights

$$\begin{aligned} g^{\ddagger}_{fc} &= g^{\ddagger}_{c} - (1-\lambda)\Delta\mu \qquad & g^{\ddagger}_{rc} &= g^{\ddagger}_{c} \\ g^{\ddagger}_{fm} &= g^{\ddagger}_{m} - \lambda\Delta\mu + w\delta \qquad & g^{\ddagger}_{rm} &= g^{\ddagger}_{m} - w\,(1-\delta), \end{aligned} \qquad [7]$$

where $g^{\ddagger}_{c}$ and $g^{\ddagger}_{m}$ are intrinsic barriers common to both the forward and reverse transitions. We have assumed that changes in λ affect the forward and not reverse barrier heights because these are the changes that will have the greatest impact on machine speed (*SI Appendix*, section 2.A).

Finally, let N define the number of mechanical substeps used by the machine. When $N = 1$, the machine has a single mechanical step (two total states illustrated in Fig. 1). For a machine with N substeps, the cycle has $2N$ total states of alternating chemical

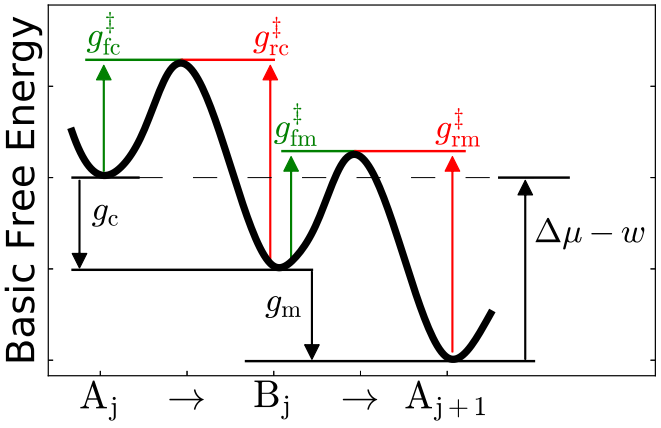

Fig. 2. The basic free-energy changes and barrier heights across a machine's landscape. For this two-state model, g_c is the basic free-energy difference from state A_i to B_i, while g_m is the basic free-energy difference from state B_i to A_{i+1}. Across the full cycle, $g_c + g_m = -\Delta\mu_{diss}$. The free-energy barriers for forward transitions are labeled in green, and the barriers for reverse transitions are in red. We explore mechanisms that have different values of g_c and g_m along with corresponding changes to the barrier heights.

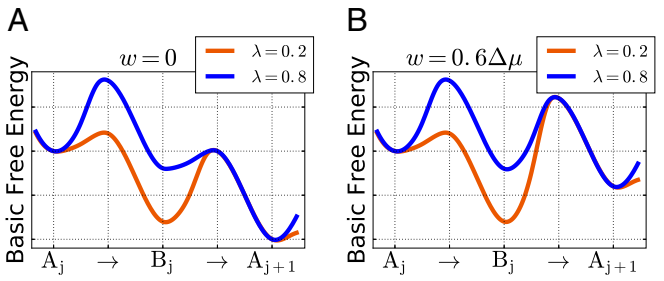

Fig. 3. The basic free-energy landscapes of two theoretical machines. The first machine (orange) has most of its basic free energy drop across the nonmechanical step, $\lambda = 0.2$. The second machine (blue) has most of its basic free energy drop across the mechanical step, $\lambda = 0.8$. Here, $g_c^{\ddagger} = g_m^{\ddagger}$. (*A*) When no work is performed, these machines have the same speed. Each machine has one small and one large barrier to traverse. (*B*) At larger values of work, the second machine ($\lambda = 0.8$, blue) is much faster. The first machine ($\lambda = 0.2$, orange) has one very small and one very large barrier to traverse, while the second machine has more evenly distributed barriers. Here, $w = 0.6\Delta\mu$.

and mechanical steps. For simplicity, we assume each of these N substeps is identical. From Eqs. **4** and **7**, $J(\Delta\mu, w)$ is the speed of a machine with a single mechanical step (two total states) and $J_{2N} = \frac{1}{N} J(\Delta\mu/N, w/N)$ is the speed of a machine with N substeps ($2N$ total states of alternating chemical and mechanical steps) (*SI Appendix*, section 2.C).

How Machines Can Optimize Speed and Efficiency

To study machine optimization, we seek ways to maximize the speed of the two-state model, at fixed efficiency, with respect to a model parameter θ by solving

$$\left.\frac{\partial J}{\partial \theta}\right|_{\eta} = 0, \qquad [8]$$

to find the optimal value θ_{opt}. Specifically, we consider $\theta \in \{\lambda, \delta, N\}$. The recent work of Brown and Sivak (10, 11) on molecular machines and other previous work on maximizing the catalytic efficiency of enzymes (12, 13) have given much insight into how to best distribute the barrier heights and state stabilities across a landscape to maximize speed. We build on this approach to address a question of evolution or synthetic design that is specific to biomolecular machines: What are the biological mechanisms that best "use" the downhill chemical input energy to overcome the large kinetic barriers of performing work?

Biological machines are impressively fast, given that the mechanical step has a large barrier that arises not only from uphill work but also from large conformational changes [the mechanical step of myosin V, for example, spans 36 nm (18)]. Intuitively, we might expect speed to decrease exponentially with respect to increasing work, $J \propto e^{-\beta w}$, based on an Arrhenius law for a single irreversible transition across the mechanical barrier, assuming this barrier height increases with the amount of work. But this is not observed; biological machines maintain high speeds while performing a large amount of work. This suggests an evolutionary optimization to be fast and efficient. Using Eq. **8**, we find the optimal parameters of our two-state model and connect them to biological mechanisms that optimize the entire speed–efficiency tradeoff; they increase speed at no cost to efficiency or vice versa.

Maximizing Machine Speed by Varying the Basic Free-Energy Drop Across the Mechanical Step. We first explore how machine speed and efficiency depend on the λ parameter, which determines the drop in basic free energy across the mechanical step. Here, for simplicity, we assume the machine has a single mechanical step ($N = 1$). Using Eq. **7** to define the barrier heights, we solve $\partial J/\partial\lambda = 0$, with all other model quantities (δ, $g_c^{\ddagger}$, $g_m^{\ddagger}$) fixed, to find λ_{opt} (*SI Appendix*, section 2.B):

$$\lambda_{\text{opt}}(\Delta\mu, w) = \frac{1}{2} + \frac{w\delta}{2\Delta\mu} + \frac{g_m^{\ddagger} - g_c^{\ddagger}}{2\Delta\mu}. \qquad [9]$$

Inserting λ_{opt} into the definitions of the barriers, Eq. **7**, gives the result that the machine operates fastest when the two barrier heights are equal, $g_{fc}^{\ddagger} = g_{fm}^{\ddagger} = 0.5\left(g_c^{\ddagger} + g_m^{\ddagger} - \Delta\mu + w\delta\right)$. This optimization principle for molecular machines is similar to the principle of Knowles, who showed for enzymes that turnover rates are maximal when the rates of binding reactants and releasing products are equal (12, 13), and the work of Brown and Sivak who, using a two-state cycle, showed that machine speed is optimized when the forward rates are equal (10).

Here is more intuition about Eq. **9**. The first term on the right-hand side of Eq. **9** ($=1/2$) shows that the chemical input free energy should be distributed evenly across the cycle, all else being equal. The second term expresses that if the machine performs much work, there is a large barrier in the mechanical step, and hence more of the available basic free energy should be expended across the mechanical step. The third term shows that the optimal distribution of basic free-energy changes will depend on the intrinsic free-energy barriers of the steps $g_c^{\ddagger}$ and $g_m^{\ddagger}$. That is, if the mechanical step has a large intrinsic barrier [e.g., from the large entropic barrier that accompanies the conformational change in myosin V's 36-nm step (18)], then more of the basic free energy should be expended in the mechanical step to reduce this intrinsic barrier. Alternatively, if the chemical barrier is intrinsically high, then less of the basic free energy should be expended in the mechanical step to achieve optimal speed.

Fig. 3 shows the landscapes of two theoretical machines. The first one (orange, $\lambda = 0.2$) has most of the total basic free-energy drop across the first, nonmechanical step. The second one (blue, $\lambda = 0.8$) has most of the basic free-energy drop across the mechanical step. When no work is performed, each machine has one small and one large barrier (Fig. 3*A*), and they have identical speeds. When work is performed, the second machine ($\lambda = 0.8$) is faster and has more evenly distributed barrier heights (Fig. 3*B*). Fig. 4 shows the speed–efficiency tradeoffs. A machine with a large decrease in basic free energy across the mechanical step (large λ) is faster at high efficiency.

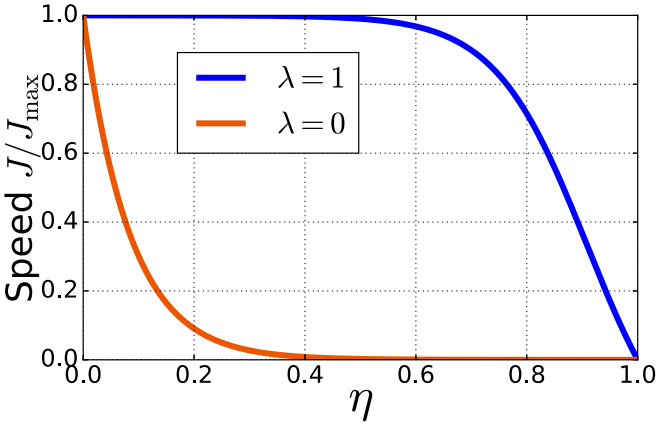

Fig. 4. The speed–efficiency tradeoffs for a machine with $\lambda = 1$ (blue) and $\lambda = 0$ (orange). The machine with a large basic free-energy drop across the mechanical step ($\lambda = 1$) is faster at high efficiency. Here, $g_c^{\ddagger} = g_m^{\ddagger}$ and $\delta = 1$.

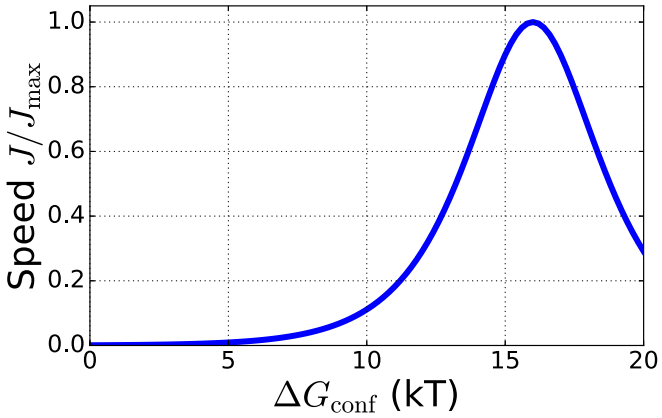

Fig. 5. To achieve maximum speed, a molecular machine has an optimal change in conformational free energy. Shown is the speed of a theoretical machine with respect to the conformational free-energy change across the mechanical step ($-\Delta G_{conf}$). Here, $\Delta\mu = 20$ kT, $w = 12$ kT, $g_c^{\ddagger} = g_m^{\ddagger}$, and $\delta = 1$.

A Conformationally Driven Mechanical Step Optimizes Speed. Here, we give a molecular interpretation of λ_{opt} from Eq. **9** in terms of a machine's conformational free-energy landscape. The idea is that, through changes in the conformational free energy, the input free energy can be stored in the machine in the first, chemical step and then expended in the mechanical step. The conformational free energy contributes to the change in basic free energy across a transition. Because changes in conformational free energy must sum to zero across a full cycle, these contributions are implicitly included in the parameter λ.

We assume here that all of the chemical free energy $\Delta\mu$ is released across the first transition. We label the change in conformational free energy across this chemical step as ΔG_{conf}. The conformational free energy across the mechanical step is then $-\Delta G_{conf}$. We expand the definition of basic free-energy changes from Eq. **6** to explicitly include these terms:

$$g_c = g_{fc}^{\ddagger} - g_{rc}^{\ddagger} = -(1-\lambda)\Delta\mu = -\Delta\mu + \Delta G_{conf}, \qquad [10]$$
$$g_m = g_{fm}^{\ddagger} - g_{rm}^{\ddagger} = -\lambda\Delta\mu + w = -\Delta G_{conf} + w.$$

Eq. **10** shows that $\lambda = \Delta G_{conf}/\Delta\mu$. So, using Eq. **9**, we can now express what conformational free energy optimizes the machine speed:

$$\Delta G_{conf,\,opt}(\Delta\mu, w) = \frac{\Delta\mu}{2} + \frac{w\delta}{2} + \frac{g_m^{\ddagger} - g_c^{\ddagger}}{2}. \qquad [11]$$

Fig. 5 shows the prediction of Eq. **11** that, under most conditions, the fastest machines will be those having a relatively large and specific value of conformational free-energy storage. The machine takes up and stores this free energy in the chemical step and expends that free energy in the mechanical step, like the cocking and releasing of a spring.

Fig. 5 shows that a machine having a suboptimal conformational change can run orders of magnitude slower. Conformational energy storage modulates the barrier heights across the machine cycle. A machine with small ΔG_{conf} would have one small barrier and one large barrier (orange curve in Fig. 3*B*). Larger conformational free-energy storage will raise the barrier of the chemical step and lower the larger barrier of the mechanical step. This serves to more evenly distribute the barrier heights (blue curve in Fig. 3*B*).

Machines Are Faster That Have an "Early" Transition State. Our model also allows for a parameter δ, which can be interpreted as the position of the transition state along the machine's mechanical step (Eq. **7**). It has been shown that machines are faster if they have a small value of δ (7, 8) and we have shown that this conclusion is general (9). That is, $\partial J/\partial\delta < 0$ under all conditions and for arbitrarily complex machine models (which include futile hydrolysis cycles, ATP-driven backsteps, etc.). A smaller value of δ (i.e., a transition state close to the initial state) always corresponds to a machine that is faster, more powerful, and more efficient at constant velocity. And it corresponds to a favorable, concave speed–efficiency tradeoff as in the blue curve in Fig. 4.

We note that a machine's power stroke, depending on how it is defined, may correspond to this optimal value of δ (8, 9, 19) or to the optimal value of λ (20, 21). We do not advocate any specific definition here, but by either definition, a power stroke may refer to the release of conformational strain across a machine's mechanical step.

Speeding up Machines with Mechanical Substeps. Machine speed can be optimized by breaking the large output step into smaller alternating chemical and mechanical steps, which we call mechanical substeps. A machine that has four 10-kT–sized barriers is faster than a machine with one 40-kT barrier. This principle applies broadly but is best illustrated for a machine where all of the chemical energy is taken up in the nonmechanical step and all of the work is performed in the forward mechanical step ($\lambda = 0$ and $\delta = 1$). Consider a set of machines that have different numbers N of mechanical substeps but that are otherwise identical. As discussed above and in *SI Appendix*, section 2.C, if $J(\Delta\mu, w)$ is the speed of a machine with a single mechanical step (two total states), then $J_{2N} = \frac{1}{N} J(\Delta\mu/N, w/N)$ is the speed of a machine with N substeps ($2N$ total states of alternating chemical and mechanical steps).

The mechanical substeps reduce and distribute the free-energy barriers of the machine, as shown in Fig. 6. Fig. 6, *Inset* shows that, when performing a large amount of work, a machine with more substeps is several orders of magnitude faster than an analogous machine with one large step. Biological machines can leverage the four separate downhill components of ATP hydrolysis (ATP binding, hydrolysis, ADP release, and P_i release) to split up their work steps. This is observed in the myosin family, where $N = 2$ for the 6-nm step of myosin II (22), and $N = 3$ for the 36-nm step of myosin V (18).

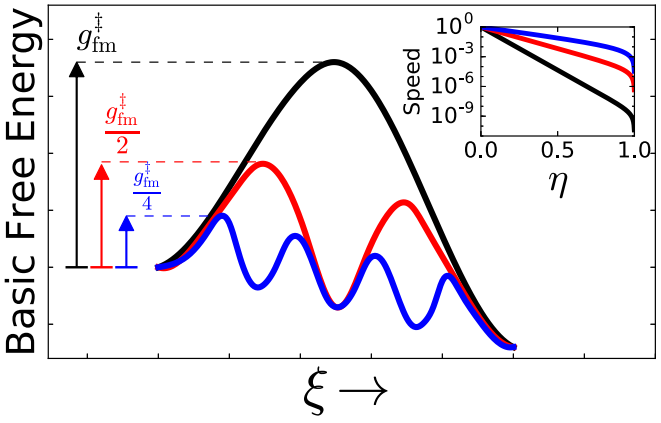

Fig. 6. Splitting one large work step (black) into two (red) or four (blue) mechanical substeps. ξ is the reaction coordinate. Modifying a molecular machine to have more substeps reduces the barrier height along the mechanical step. *Inset* shows that, when performing a large amount of work, a machine with several mechanical substeps can be several orders of magnitude faster than a machine with a single mechanical step. Speed is plotted on a log scale.

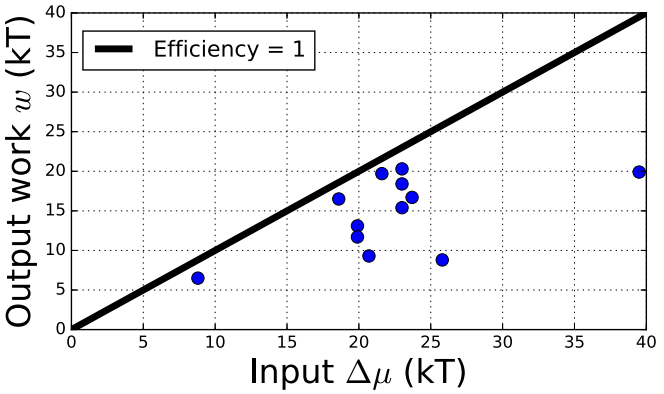

Fig. 7. The in vivo efficiencies of molecular machines. Included are Na-K ATPase; SERCA; the proton PPi pump; the plasma membrane proton pump; PMCA; V-ATPase; myosin II; NCX; NCKX; and animal, *Escherichia coli*, and chloroplast F_oF_1-ATPase. The efficiency $\eta = w/\Delta\mu$, where these values of $\Delta\mu$ and w are calculated from experimental data (*SI Appendix*, section 3).

Similarly, F_oF_1-ATPase uses mechanical substeps. In a recent study, Anandakrishnan et al. (6) used a simple kinetic model to study the evolutionary optimization of this motor. Their work shows that the rotary mechanism of F_oF_1-ATPase optimizes speed with the same principle described here for mechanical substeps—the rotary mechanism reduces and distributes the kinetic barriers of the machine cycle. This motor takes, as input, the downhill transport of 8–15 protons, depending on the species (23). The rotary mechanism intersperses these downhill steps with the synthesis of three ATP molecules (output), each of which is further subdivided into separate work steps of reactant binding, synthesis, and product release (24, 25). This gives a more even application of torque across the angular coordinate of the motor (5).

Other biological machines also use mechanical substeps. In *SI Appendix*, section 2.C, we use Eq. **8** to calculate N_{opt} for different machines and to discuss various practical considerations.

Biological Machines Are Both Fast and Efficient. Fig. 7 shows that biomolecular machines in vivo tend to have high efficiencies. For many machines, these in vivo values of input free energy $\Delta\mu$ and output work w used to calculate efficiency will vary, depending on cell conditions. But for the machines in Fig. 7, these values are known under typical conditions and appear to be fairly consistent (*SI Appendix*, section 3). These machines are as efficient as macroscopic electric motors and more efficient than heat engines; $\eta > 50\%$ for 10 of the 12 machines shown.

Fig. 8 shows the speed–efficiency relationships for various biomolecular machines as measured from in vitro experiments. These machines have tradeoff curves that are much more favorable than would occur in a single Arrhenius barrier process, also shown for reference.

We now rationalize some of the differences in the speed–efficiency behaviors shown in Fig. 8. (We do not discuss F_1-ATPase because these speed–efficiency data, obtained for the isolated F_1 domain running in the hydrolysis direction, do not match the motor's in vivo function.) Consistent with the model, machines with the best speed–efficiency curves in Fig. 8 have more substeps, N. And these machines all have large values of λ, except for RNAP, which has the worst speed–efficiency tradeoff. Kinesin and dynein also have small values of δ, the transition-state location. See *SI Appendix*, section 4 for the values of N, λ, and δ (estimated from model fits to the in vitro single-molecule data from Fig. 8).

Na-K ATPase has the best speed–efficiency tradeoff of the machines in Fig. 8. This pump hydrolyzes ATP as input to export three Na^+ ions from the cell and import two K^+ ions uphill against their chemiosmotic gradients. This machine has such a good tradeoff because the output work is delocalized across the entire cycle and therefore the rate-limiting work step (the release of one of the Na^+ ions) is only weakly dependent on the total work of the machine (26). This pump effectively has many substeps, although we do not report an exact value since it is difficult to estimate the work contribution over the various transitions (the occlusion, transport, and release of each of the five ions).

The cytoskeletal transport motors myosin V, kinesin, and dynein are fast at high efficiency, but they have fewer substeps than Na-K ATPase [$N = 3$ for myosin V (18)]. The tradeoffs of these three motors may also be affected by the run length L, the average number of full cycles a motor completes before falling off its cytoskeletal track. At zero load, $L \approx 25$ for myosin V (27), $L \approx 100$ for kinesin (28), and $L \approx 250$ for dynein (29). For these three motors, the trend in L (dynein > kinesin > myosin V) is anticorrelated with the speed–efficiency behavior (myosin V > kinesin > dynein). It is possible that the motor's run length introduces an extra tradeoff, where different biological mechanisms can use the available free energy to achieve a greater run length, but at the expense of speed or efficiency.

RNAP has the worst speed–efficiency behavior of the machines in Fig. 8. RNAP synthesizes RNA from a template DNA strand (30). As output work, RNAP generates force that melts the DNA template. This output work is physically separated from the machine itself—RNAP breaks hydrogen bonds that are several base pairs upstream from the motor (31). This physical separation may make it difficult or impossible for RNAP to use the speed-optimizing strategies we have described. The motor does not use mechanical substeps and it has a small value of $\lambda = 0.22$, in agreement with the observation that it operates as a Brownian ratchet (30).

Conclusions

We have explored the optimization of speed and efficiency of molecular machines using a simple dynamical model. Our model explores parameters of evolution and synthetic design: not just what is, but what could have been. We find that, at high efficiency, a machine's speed can be increased several orders of magnitude by coupling the downhill chemical input to the uphill work through an intermediate conformational change and by breaking the large kinetic barrier of a single work step into

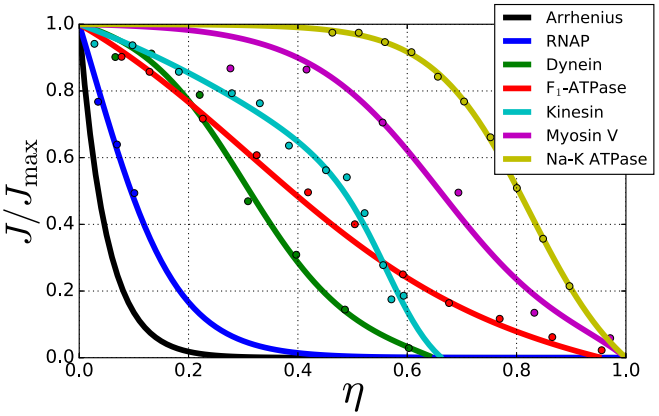

Fig. 8. The speed–efficiency relationships for six molecular machines. Speed is normalized with respect to the maximum speed of each machine. These machines maintain a high speed even while operating at high efficiency. The black line shows a reference model of a single-barrier, irreversible, Arrhenius process. Data are from refs. 30 and 32–36. Fits to the data are described in *SI Appendix*, section 4.

multiple smaller substeps. The benefit of these mechanisms can be seen in the experimentally determined speed–efficiency tradeoffs of biological machines: They allow machines to maintain a high speed even at high efficiency.

These principles are broadly applicable to molecular machines. But one—the optimal value of λ, the basic free-energy drop across the mechanical step—depends on the amount of work that is performed. Some machines operate under fairly consistent loads or forces, but others undoubtedly experience a range of loads. Although we do not explore it here, it is interesting to consider what machine mechanisms may have evolved to optimize performance over such varying conditions.

ACKNOWLEDGMENTS. We thank Dean Astumian, Dan Zuckerman, and Joe Howard for comments and suggestions. We are grateful for support from the Laufer Center for Physical and Quantitative Biology and from NIH Grant GM06359217.

1. Dimroth P, von Ballmoos C, Meier T (2006) Catalytic and mechanical cycles in F-ATP synthases: Fourth in the cycles review series. *EMBO Rep* 7:276–282.
2. Törnroth-Horsefield S, Neutze R (2008) Opening and closing the metabolite gate. *Proc Natl Acad Sci USA* 105:19565–19566.
3. Matsuno-Yagi A, Hatefi Y (1988) Estimation of the turnover number of bovine heart FoF1 complexes for ATP synthesis. *Biochemistry* 27:335–340.
4. Silverstein TP (2014) An exploration of how the thermodynamic efficiency of bioenergetic membrane systems varies with c-subunit stoichiometry of F_1F_0 ATP synthases. *J Bioenerg Biomembr* 46:229–241.
5. Oster G, Wang H (2000) Reverse engineering a protein: The mechanochemistry of ATP synthase. *Biochim Biophys Acta* 1458:482–510.
6. Anandakrishnan R, Zhang Z, Donovan-Maiye R, Zuckerman DM (2016) Biophysical comparison of ATP synthesis mechanisms shows a kinetic advantage for the rotary process. *Proc Natl Acad Sci USA* 113:11220–11225.
7. Schmiedl T, Seifert U (2008) Efficiency of molecular motors at maximum power. *EPL Europhys Lett* 83:30005.
8. Howard J (2011) Motor proteins as nanomachines: The roles of thermal fluctuations in generating force and motion. *Biological Physics, ed* Rivasseau V (Springer, Basel), pp 47–59.
9. Wagoner JA, Dill KA (2016) Molecular motors: Power strokes outperform Brownian ratchets. *J Phys Chem B* 120:6327–6336.
10. Brown AI, Sivak DA (2017) Allocating dissipation across a molecular machine cycle to maximize flux. *Proc Natl Acad Sci USA* 114:11057–11062.
11. Brown AI, Sivak DA (2018) Allocating and splitting free energy to maximize molecular machine flux. *J Phys Chem B* 122:1387–1393.
12. Albery WJ, Knowles JR (1976) Evolution of enzyme function and the development of catalytic efficiency. *Biochemistry* 15:5631–5640.
13. Albery WJ, Knowles JR (1977) Efficiency and evolution of enzyme catalysis. *Angew Chem Int Ed Engl* 16:285–293.
14. Hill TL, Eisenberg E (1981) Can free energy transduction be localized at some crucial part of the enzymatic cycle? *Q Rev Biophys* 14:463–511.
15. Hill T (1977) *Free Energy Transduction in Biology: The Steady-State Kinetic and Thermodynamic Formalism* (Academic, New York).
16. Seifert U (2011) Stochastic thermodynamics of single enzymes and molecular motors. *Eur Phys J E* 34:26.
17. Seifert U (2012) Stochastic thermodynamics, fluctuation theorems and molecular machines. *Rep Prog Phys* 75:126001.
18. Cappello G, et al. (2007) Myosin V stepping mechanism. *Proc Natl Acad Sci USA* 104:15328–15333.
19. Howard J (2006) Protein power strokes. *Curr Biol* 16:R517–R519.
20. Astumian RD (2016) Optical vs. chemical driving for molecular machines. *Faraday Discuss* 195:583–597.
21. Astumian RD, Mukherjee S, Warshel A (2016) The physics and physical chemistry of molecular machines. *ChemPhysChem* 17:1719–1741.
22. Capitanio M, et al. (2006) Two independent mechanical events in the interaction cycle of skeletal muscle myosin with actin. *Proc Natl Acad Sci USA* 103:87–92.
23. Pogoryelov D, et al. (2012) Engineering rotor ring stoichiometries in the ATP synthase. *Proc Natl Acad Sci USA* 109:E1599–E1608.
24. Watanabe R, Iino R, Noji H (2010) Phosphate release in F1-ATPase catalytic cycle follows ADP release. *Nat Chem Biol* 6:814–820.
25. Suzuki T, Tanaka K, Wakabayashi C, Saita E-i, Yoshida M (2014) Chemomechanical coupling of human mitochondrial F1-ATPase motor. *Nat Chem Biol* 10:930–936.
26. Castillo JP, et al. (2011) Energy landscape of the reactions governing the Na^+ deeply occluded state of the Na^+/K^+-ATPase in the giant axon of the Humboldt squid. *Proc Natl Acad Sci USA* 108:20556–20561.
27. Baker JE, et al. (2004) Myosin V processivity: Multiple kinetic pathways for head-to-head coordination. *Proc Natl Acad Sci USA* 101:5542–5546.
28. Andreasson JOL, et al. (2015) Examining kinesin processivity within a general gating framework. *eLife* 4:e07403.
29. Reck-Peterson SL, et al. (2006) Single-molecule analysis of dynein processivity and stepping behavior. *Cell* 126:335–348.
30. Abbondanzieri EA, Greenleaf WJ, Shaevitz JW, Landick R, Block SM (2005) Direct observation of base-pair stepping by RNA polymerase. *Nature* 438:460–465.
31. Wang H-Y, Elston T, Mogilner A, Oster G (1998) Force generation in RNA polymerase. *Biophys J* 74:1186–1202.
32. Visscher K, Schnitzer MJ, Block SM (1999) Single kinesin molecules studied with a molecular force clamp. *Nature* 400:184–189.
33. Toyabe S, Watanabe-Nakayama T (2011) Thermodynamic efficiency and mechanochemical coupling of F1-ATPase. *Proc Natl Acad Sci USA* 108:17951–17956.
34. Toba S, Watanabe TM, Yamaguchi-Okimoto L, Yano Toyoshima Y, Higuchi H (2006) Overlapping hand-over-hand mechanism of single molecular motility of cytoplasmic dynein. *Proc Natl Acad Sci USA* 103:5741–5745.
35. Mehta AD, et al. (1999) Myosin-V is a processive actin-based motor. *Nature* 400: 590–593.
36. Nakao M, Gadsby DC (1989) [Na] and [K] dependence of the Na/K pump current-voltage relationship in Guinea pig ventricular myocytes. *J Gen Physiol* 94: 539–565.